Granular Matter (2010) 12:527–541
DOI 10.1007/s10035-010-0211-x

Comprehensive study of the effects of rolling resistance on the stress–strain and strain localization behavior of granular materials

Abdalsalam Mohamed · Marte Gutierrez

Received: 27 February 2010 / Published online: 12 September 2010

Abstract This paper presents the results of a comprehensive study of the effects of rolling resistance on the stress–strain and strain localization behavior of granular materials using the discrete element method. The study used the Particle Flow Code (PFC) to simulate biaxial compression tests in granular materials. To study the effects of rolling resistance, a user-defined rolling resistance model was implemented in PFC. A series of parametric studies was performed to investigate the effects of different levels of rolling resistance on the stress–strain response and the emergence and development of shear bands in granular materials. The PFC models were also tested under a range of macro-mechanical parameters and boundary conditions. It is shown that rolling resistance affects the elastic, shear strength and dilation response of granular materials, and new relationships between rolling resistance and macroscopic elasticity, shear strength and dilation parameters are presented. It is also concluded that the rolling resistance has significant effects on the orientation, thickness and the timing of the occurrence of shear bands. The results reinforce prior conclusions by Oda et al. (Mech Mater 1:269–283, 1982) on the importance of rolling resistance in promoting shear band formation in granular materials. It is shown that increased rolling resistance results in the development of columns of particles in granular materials during strain hardening process. The buckling of these columns of particles in narrow zones then leads to the development of shear bands. High gradients of particle rotation and large voids are produced within the shear band as a result of the buckling of the columns.

A. Mohamed · M. Gutierrez (✉)
Colorado School of Mines, Division of Engineering, 1610 Illinois St., BB 269, Golden, CO 80401, USA
e-mail: mgutierr@mines.edu

Keywords Discrete element modeling · Granular materials · Rolling resistance · Strain localization · Stress–strain

1 Introduction

Numerous studies have been performed on the stress–strain response of granular materials particularly their strain localization behavior using analytical and numerical models as well as experimental investigations. Most of these studies are based on continuum mechanics approaches and cannot take into consideration the micro-mechanical factors that control macroscopic behavior. On the other hand, researchers have widely utilized micromechanical modeling techniques, particularly the use of Discrete Element Method (DEM), to investigate the role of particle interactions in the behavior of granular materials. DEM models have examined the effects of microscopic parameters on the macroscopic response of granular materials. The main premise in DEM is that granular materials interact at contact points between particles, and this interaction plays a dominant role in the microscopic response of granular materials [2,3]. DEM modeling is particularly suited to the study of the strain localization response of granular soils as they can take into consideration the micromechanical factors that lead to strain localization. DEM models have shown that particle size, shape, distribution, and contact stiffness and friction are all important factors in the initiation and growth of shear bands, and on the macroscopic structure of shear bands such as their thicknesses and orientations [4–7].

Strain localization is one of the most important phenomena occurring in granular materials. Strain localization occurs due to instability and bifurcation in the stress–strain response of materials during loading. The localization of deformation

in materials was first treated as a bifurcation problem by [8–10]. According to bifurcation theory, a material which undergoes homogeneous deformation can reach a bifurcation point at which the material experiences instability and deformation starts to become non-homogenous. Non-homogeneous deformation results from localized deformation, and since the predominant yielding mechanism for soils is shearing, the localized deformation zone is called a shear band. An important prediction from bifurcation theory is that for strain hardening materials, strain localization and instability can occur before the peak shear strength corresponding to homogeneous response is reached. Localization is then followed by strain softening characterized by reduction in load carrying capacity during continued deformation. Beyond the bifurcation point, the observed response can no longer be considered as material response for calibrating constitutive models because the response corresponds to non-homogenous deformation.

Granular materials are ensembles of particles which interact at contact points. Each particle can move relative to neighboring particles by sliding and/or rolling at contact points. However, in classical continuum mechanics, sliding is considered to play the dominant role in microscopic deformation of granular materials. For example, the shear strength and dilatancy of granular soils have been explained to be mainly due to pure sliding [11–13]. Particles are assumed to be perfectly circular, and to rotate freely and offer no resistance to rotation. In reality, real particles are non-circular and have rough surface textures [14], and particles could not roll freely when in contact with other particles. Rolling resistance can be defined as a force couple that is transferred between the particles through the contacts, and this force couple inhibits particle rotation. Rolling resistance has been used in DEM as a simple way of modeling the effects of non-circular and irregular particle shapes on contact behavior [5,15]. Bardet [16] compared the stress–strain response of granular materials under two assumptions: fixed and free rotation. It was found that the initial Young's modulus of a granular material was not affected by particle rotation, while the peak and residual friction angles, and the dilation angle were larger with fixed rotation than with free rotation. Wang et al. [17] have showed that particle rolling resistance reduces the post-peak oscillations that occur in DEM simulation of the stress–strain behavior of granular materials.

Recent experimental studies have looked at the microstructural behavior of granular materials by means of X-ray and other imaging techniques. It has been observed that rolling, rather than sliding, dominates the microscale deformation of granular media [1]. Oda and Iwashita [18] showed that rolling resistance has a very important effect on the DEM simulation of shear band formation in granular materials. It was shown that rolling resistance promotes shear band formation in granular soils. Microstructural observations from experiments on shear band formation in granular soils show that particles rotate extensively inside the shear band resulting in high particle rotation gradients along the band boundaries [5,19]. Due to the gradient in particle rotations, columns of vertical chains of particles buckle along the shear band. Rotational resistance prevents chains of particles from completely collapsing due to buckling [7]. As result of localized buckling of columns of particles, large shear strain concentrations are accompanied by local large voids of particles inside the shear band. Oda et al. [20], and Oda and Kazama [21] reported that realistic DEM modeling of high particle rotations and large voids inside shear bands can only be accomplished by considering rolling resistance at contact points in such modeling. Tordesillas and Shi [22] have reported that the strain level at bifurcation increases and the shear band width decreases with increasing rolling resistance.

Several recent studies have conclusively shown that rolling resistance is a significant parameter influencing the stress–strain and strain localization response of granular materials. However, these studies have been conducted using a limited range of values of rolling resistance, parameters and boundary conditions. Thus, it has nor been possible to fully quantify the effects of rolling resistance. The main objective of this paper is to present the results of a comprehensive study using DEM modeling of the effects of the variation in rolling resistance on the elasticity, shear strength, dilation and bifurcation response of granular materials. A comprehensive parametric study is performed whereby the magnitude of rolling resistance is varied within its full range of possible values in conjunction with variations in other model parameters and boundary conditions.

2 Methodology

2.1 DEM overview

The comprehensive study of the effects of rolling resistance on the stress–strain and strain localization response of granular materials was performed using DEM and the two-dimensional computer code PFC (particle flow code) developed by [23]. PFC models granular materials using distinct rigid spherical or disk-shaped particles that interact only at contacts or interfaces between the particles. In DEM, mechanical behavior is expressed in terms of the movements of each particle and the internal forces generated at each contact point. Newton's second law of motion provides the fundamental relationship between particle motion and the forces causing that motion. PFC uses an explicit time-stepping algorithm that requires the repeated application of the second law of motion for each particle, a force-displacement law for each contact, and the constant updating of the wall positions. Contacts, which may exist between two particles

or between a particle and a wall, are formed and broken automatically during the course of a simulation. For quasi-static loading, artificial damping is introduced to eliminate the transient displacements and achieve a steady-state solution.

A central component of a DEM model is the contact law used for the interactions between particles. Several such models are available and they account for different types of interactions such as contact stiffness, slip and bonding [23]. The stiffness models relate the contact forces and relative displacements in the normal and shear directions. The incremental normal contact force N_i and shear force T_i are calculated from the incremental normal displacement U_i^n and shear displacement U_i^s, respectively, by:

$$\Delta N_i = K^n \Delta U_i^n, \quad \Delta T_i = K_i^s \Delta U_i^s \tag{1}$$

where K^n and K^s are the tangential normal and shear stiffnesses, respectively. The contact stiffnesses used in the above equations are assigned different values depending upon the contact-stiffness model employed. PFC provides two types of contact-stiffness models: a linear model, and a simplified nonlinear Hertz-Mindlin model. In addition to the normal stiffness, the magnitude of interpenetration or overlap between particles is controlled by a limiting contact overlap value.

The slip model describes the constitutive behavior tangential to the particle contact between two particles. It is defined by the friction coefficient μ at the contact, where μ is taken to be the friction coefficient of the two contacting entities (particle-to-particle, or particle-to-wall). Slip between particles at a contact i is allowed to occur only if the following condition is satisfied:

$$T_i = \mu N_i \tag{2}$$

Contact-bond at particle contacts is analogous to applying glue at the contact. The presence of contact bond precludes the possibility of slip unless the bond strength is exceeded and the bond is destroyed. A contact bond is defined by a normal contact bond strength N_c and the shear contact bond strength T_c. If the magnitude of tensile normal contact force equals or exceeds the normal bond strength (i.e., $N_i = N_c$), the bond breaks, and both the normal and shear forces are set to zero. On the other hand, if the magnitude of the shear contact force equals or exceeds the shear contact bond strength (i.e., $T_i = T_c$), the bond breaks, but the contact forces are not changed.

Built-in contact models can be modified or new contact models can be conveniently introduced in PFC by writing and coding a user-defined model (UDM) in C++. The C++ program, compiled as a DLL (dynamic link library), makes it easy to add new models in PFC. The C++ file contains the function that implements the new model, and once the model is installed, the host program can refer to the specific model's name in PFC commands. Furthermore, the model and its associated properties can be manipulated by PFC's built-in language FISH in a similar way in which other built-in functions are used by PFC. This capability to program new contact models is exploited below in the introduction of a rolling resistance model in PFC.

2.2 Implementation of rolling resistance in DEM

In conventional DEM, particle rolling occurs without any resistance. The granular medium is assumed to be an assembly of discrete particles and the mechanical relationships between particles are determined by normal spring, tangential spring and friction parameters. However, as mentioned, in reality particles contact each other on surfaces with finite area and, thus, a moment of rolling resistance exists when a particle rolls over another. Bardet and Huang [24] introduced the first model for the rolling resistance between particles based on experiments using rolling cylinder particles placed between two rigid plates. Iwashita and Oda [25] implemented the first complete model on the rolling resistance of granular particles in DEM. In the model by [25], a rotational spring and rolling dashpot are installed between the particles. When compression occurs, the conventional normal contact relation is applied, and when the particles begin to rotate relative to each other, the rotational model is applied. The rotational model used in this study is briefly described below.

The contact force F_i, which represents the action between two particles at the ith contact, may be decomposed into a normal component N_i and a shear component T_i. Two types of kinematical behavior can occur for a contact: sliding and/or rolling. Sliding starts working at contact point when N_i and T_i satisfy the condition given in Eq. (2). On the other hand, the conservation law of angular momentum for a single particle expressed by the following equation describes the rolling motion of a particle:

$$\sum_{i=1}^{m} (T_i r + M_i) = I \frac{\partial w}{\partial t} \tag{3}$$

where M_i is the rotational moment acting on the particle's centroid, and I and w are the polar moment of inertia and angular velocity of the particle, respectively. The rolling resistance model consists of an elastic spring, a dashpot, a no-tension joint and a slider which provides two sources of rolling resistance. The elastic rotational force-displacement relation is described by the following equation:

$$M_i = K_r \theta_r \tag{4}$$

where θ_r is the relative rotation between two particles and K_r is the rolling stiffness and its value for small displacements is obtained as [24]:

$$K_r = 2r N_i J_n \tag{5}$$

The parameter J_n varies from 0.25 to 0.5 depending on the roundness of the particle. Since perfectly rigid spherical particles are used in this study, a fixed value 0.5 is used for J_n for all simulations.

Rolling starts working when M_i exceeds the threshold value of ηN_i:

$$|M_i| > \eta N_i \tag{6}$$

where η is a rolling resistance parameter with a dimension of length. Once the resistance is exceeded, the particle begins to roll without mobilizing any further rolling resistance. Note that $\eta = \beta B$, where B is equal to half of contact width between two particles. The interface/contact width B is dependent on the shape parameter δ and the common radius r [2], and therefore:

$$\eta = \delta r \beta = \alpha r \tag{7}$$

For two contacting particles A and B with different radii r_A and r_B, the common radius r is defined by the geometric mean radius of the two contacting particles:

$$r = \frac{2 r_A r_B}{r_A + r_B} \tag{8}$$

Alternatively by using Eq. (7), Eq. (6) can also be re-written as:

$$|M_i| > \eta N_i = \alpha r N_i \tag{9}$$

where α is combination of two dimensionless constants β and δ. The parameter α, which depends totally on the distribution of contact force at the contact surface, is called the *rolling friction coefficient*. The physical meaning of α is analogous to the inter-particle friction coefficient μ [26], and it controls how much rolling resistance can be generated at any contact point.

Several researchers have improved on the work of [5] and [25] and have developed more comprehensive models of rolling resistance for granular materials. A complete model of rolling resistance, which accounts for both rolling and sliding in a more theoretical framework based on local equilibrium condition, was proposed by [15]. This model also used a contact width B, which depends on the grain size, and a shape parameter δ, which takes a value of 0 for no rolling resistance, and 0.1–1.6 for materials with rolling resistance. It should be noted that the shape parameter δ is also partly accounted for in the rolling friction coefficient α in Eq. (9). Jiang and Harris [27] introduced new kinematic variables for relative and pure rotation rates in order to narrow the gap between DEM and continuum modeling of granular materials. To account for the contribution of surface roughness of particles to rolling resistance, [28] developed a simple micro-model for capturing the roughness of particles by discretizing the contact width between particles into a finite number of basic elements, with each basic element having spring, dashpot and slider components. Equations governing the motion of particles based on local equilibrium were derived to establish normal, tangential and rolling models. Other rolling resistance models that have been developed are those of [29] for bonded granular materials, and [30,31] for frictional powders. Finally, models for rolling resistance as well as torque resistance for 3D DEM simulation have been proposed by [30,32].

Although more comprehensive models for rolling resistance are available, the study presented in this paper used the original formulation of [5] and [25] in order to limit the number of variables involved to one basic model parameter, namely the rolling friction coefficient. In this way, the parametric study can be carried out systematically without the complications of having to deal with multiple model parameters. Future studies should consider the effects of other parameters such as particle surface roughness and bonding. The rolling resistance model described above was implemented as a user defined model (UDM) in PFC. This model and the parameter α are used in the parametric study of the stress–strain and strain localization behavior of granular materials.

2.3 DEM modeling

The comprehensive investigation of the effects of rolling resistance on the strain localization response of granular materials is performed under two-dimensional biaxial loading conditions. The biaxial model is rectangular, 12 cm high and 6 cm wide, and consists of an assembly of poly-dispersed disk-like particles (Fig. 1). Three ranges of particle radii were used: (1) 0.3–0.4 mm, (2) 0.3–0.6 mm and (3) 0.3–0.8 mm. For these particle radii, the size of the model is deemed large enough to simulate a representative element volume of granular material, but not too large to require prohibitive calculation times. The sample is contained by four frictionless walls. The top and bottom boundaries are loaded by rigid platens and by the major principal stress σ_1. The left and right lateral walls are confined also by semi-rigid walls and by the minor principal stress σ_3. The sample is first loaded isotropically during consolidation, then sheared by increasing the vertical strain until the peak and post peak shear stress have been achieved. Shearing is performed under constant vertical strain rate $d\varepsilon_1/dt$ of 0.05 m/min and constant horizontal or confining stress σ_3. The top and bottom platens move in the vertical direction toward each other under a strain-controlled condition. The velocity of the lateral walls is controlled automatically by a numerical servo-control program so as to maintain a constant confining pressure.

To generate the model, a random particle generation procedure called the "expansion method" [23] is adapted to achieve a desired sample particle size distribution and porosity. The expansion method employs a constant factor,

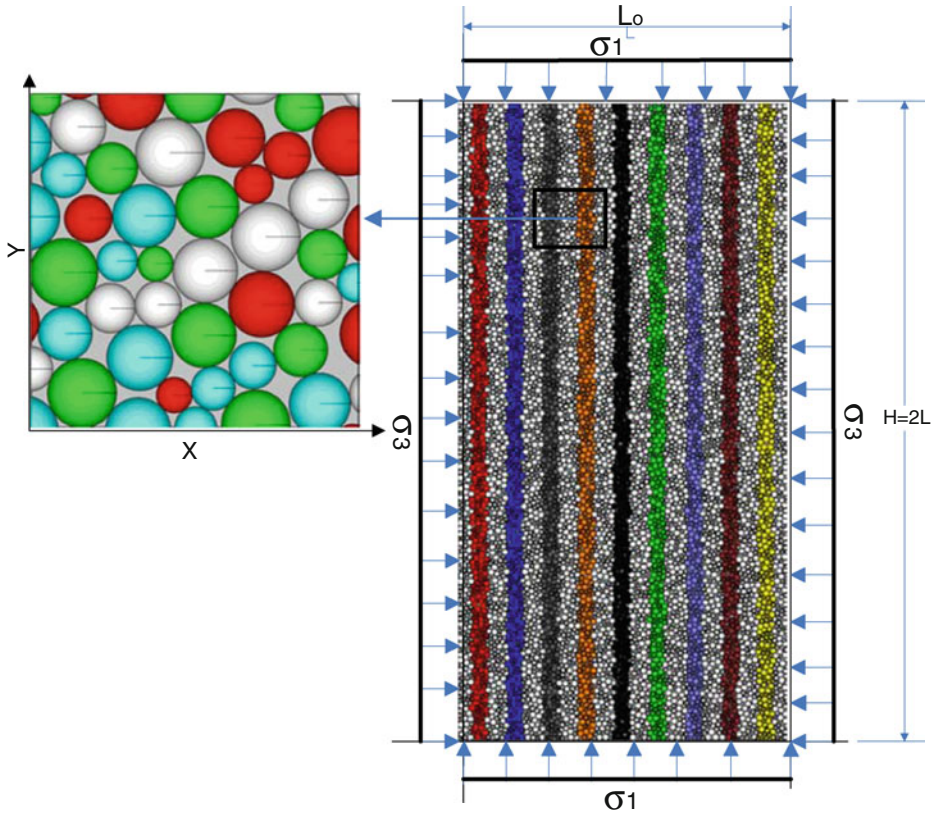

Fig. 1 Set-up of the biaxial DEM model for the simulation of the stress–strain and strain localization response of granular materials

expressed as a multiple of the particle radii, which is adjusted and the particle sizes are increased until the system reaches an equilibrium state after some calculation cycles. Due to the particle radii expansion, particles greatly overlap and thus strong repulsive forces are developed at the contacts. Cycling is required to achieve equilibrium between the unbalanced contact forces and the forces generated by the isotropic boundary stresses from consolidation.

The model parameters values used in the study are summarized in Table 1. The main material parameters (i.e., density ρ, normal stiffness K_n and friction coefficient μ) are similar to those used by [33] in the DEM simulation of the stress–strain behavior of granular materials. Some of the parameters were given a range of values to test the sensitivity of model response to changes in parameter values. The shear stiffness K_s is assumed to be a constant ratio of K_n and different ratios of the shear stiffness to normal stiffness K_s/K_n were used in the simulations (in comparison [33] assumed K_s and K_n to be equal). Except when otherwise noted, the results presented below are for the base case of $\mu = 0.5, \sigma_3 = 1$ MPa and $K_s/K_n = 1$. The lateral walls were given a stiffness that is 1/10th of the particle-to-particle contact stiffness in order to simulate a semi-rigid confining membrane. The biaxial tests were run for range of confining pressures with σ_3 varying from 0.1 to 10 MPa. It is known in the literature that a DEM model with more than 5,000 particles provides a representative element volume for the modeling of the stress–strain response of granular materials. In this study, the number of randomly generated particles ranged from 6,556 to 16,190 (Table 1).

To track the development of shear bands in the biaxial tests, a series of equally spaced particle columns were given contrasting colors before shearing. Each of these columns, which run from top to bottom, has a width of three particles. A typical profile of columns in a 60 mm wide sample is shown Fig. 1. The colors were used only to clarify the buckling of particles column during shearing and have no effect on the simulation results. Additionally, to track their rotations, the particles were marked by a horizontal radial line before shearing as shown Fig. 1. These lines will rotate clockwise or counter-clockwise as particles start rolling after shearing.

The rolling friction coefficient α is affected by the particle shape, normal stiffness and normal force at a point of contact and its value typically ranges from 0 to 1. For $\alpha = 0$, no rolling resistance (i.e., free rolling) exists at a contact point. Based on a preliminary analysis, particle rotation is effectively prevented (i.e., no rolling) when $\alpha = 1$. As noted above, α is analogous to the friction coefficient μ and, thus, a value of $\alpha = 1$ is equivalent to prescribing a high rolling friction angle. Therefore, parameter α is given values

Table 1 Model parameter values used in the DEM simulations

Model parameters	Values		
Sample dimensions (cm)	Height: 12, Width: 6		
Particles sizes (mm)	0.3–0.4	0.3–0.6	0.3–0.8
Number of particles	16,190	9,794	6,556
Porosity, n	0.10	0.13	0.16
Particle density, ρ (kg/m^3)	2,630		
Inter-particle friction coefficient, μ	0.5, 0.6, 0.7		
Contact normal stiffness, K_n (N/m)	$5 \cdot 10^8$		
Ratio of shear and normal stiffnesses, K_s/K_n	0.1, 0.25, 0.5, 1.0, 2.0, 3.0, 4.0		
Wall stiffness, K_w (N/m)	$5 \cdot 10^7$		
Particle rolling resistance, α	0, 0.001, 0.01, 0.1, 0.2, 0.5, 1.0		
Confining stress, σ_3 (MPa)	0.1, 0.5, 1.0, 5.0, 10.0		

between 0 and 1 in the simulations presented below. Table 1 list the specific values of α in conjunction with the other model parameters used in the simulations.

3 Results and discussion

3.1 Effects of rolling resistance on elastic behavior

The stress–strain response of the modeled granular material under biaxial loading conditions are shown in terms of the shear stress $(\sigma_1 - \sigma_3)$ vs. axial strain ε_1 curves in Fig. 2a for different values of the rolling friction coefficient α. Except for α, all other values of the model parameters, confining stresses and initial porosities are kept the same and these values are given in Table 1. It can be seen that the initial slopes of the stress–strain curves are the same for all values of α. It appears that the Young's modulus of the modeled granular material is not affected by the rolling resistance. This observation is in agreement with that of [16,17].

Figure 2b shows the volumetric strain ε_v vs. axial strain ε_1 response of the modeled granular material as function of α corresponding to the shear stress–strain response curves shown in Fig. 2a. The volumetric strain increment is defined as $d\varepsilon_v = (d\varepsilon_1 + d\varepsilon_3)$ where ε_3 is the lateral strain. Like the $(\sigma_1 - \sigma_3)$ vs. ε_1 curves, the initial portions of the ε_v vs. ε_1 curves are very similar and are unaffected by the rolling friction coefficient α. This indicates that the elastic Poisson's ratio ν of the modeled granular material is independent of α.

Previous studies have shown the important effects of the ratio of the shear stiffness to normal stiffness K_s/K_n on the stress–strain response of particulate models of granular

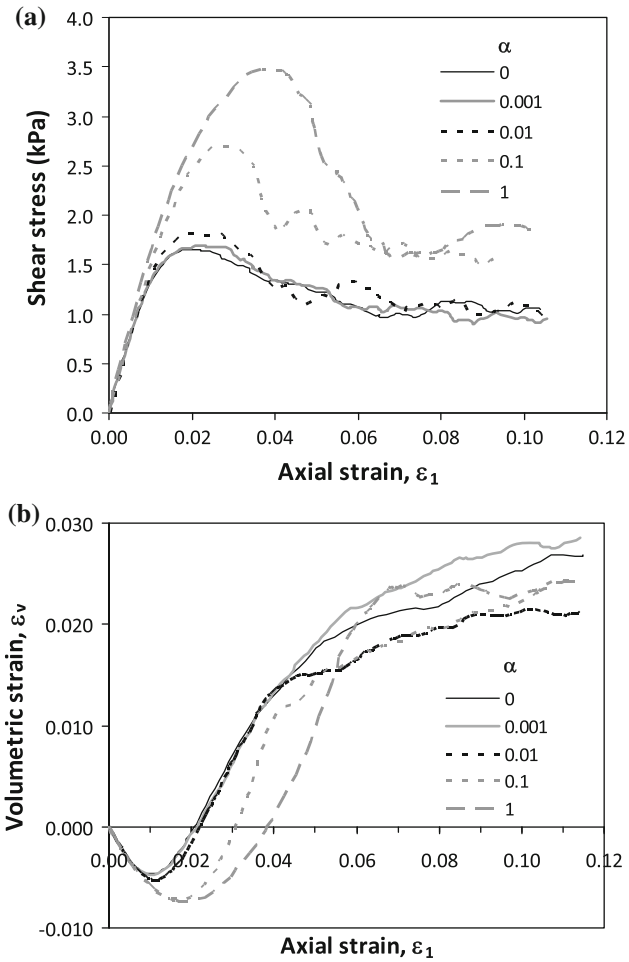

Fig. 2 Effects of the rolling friction coefficient α on the **a** shear stress–strain and **b** volumetric strain response of granular materials under biaxial loading condition

materials [34]. Thus, several values of K_s/K_n were used in the simulations as shown in Table 1. Figure 3a shows the combined effects of α and K_s/K_n on the elastic Young's modulus E of the simulated material normalized by the particle-to-particle normal stiffness K_n. It can be seen that E/K_n increases from about 0.18 for $K_s/K_n = 0.1$ to about 0.36 for $K_s/K_n = 4$. A common assumption used in the particulate modeling of granular materials is that $K_s/K_n = 1$ and this corresponds to $E/K_n \approx 0.3$. The effect of the rolling friction coefficient α on the normalized Young's modulus is very minimal.

The stiffness ratio K_s/K_n has also significant effects on the Poisson's ratio ν which decreases as the K_s/K_n ratio is increased, from $\nu \approx 0.38$ for $K_s/K_n = 0.1$ to $\nu \approx 0.13$ for $K_s/K_n = 4$. For $K_s/K_n = 1$, the Poisson's ratio is $\nu \approx 0.25$, which is a typical value obtained from experiments on granular materials. This value is different from the zero Poisson's ratio for $K_s/K_n = 1$ obtained by [34] for bonded granular materials. Also, Fig. 3b suggests that the Poisson's ratio

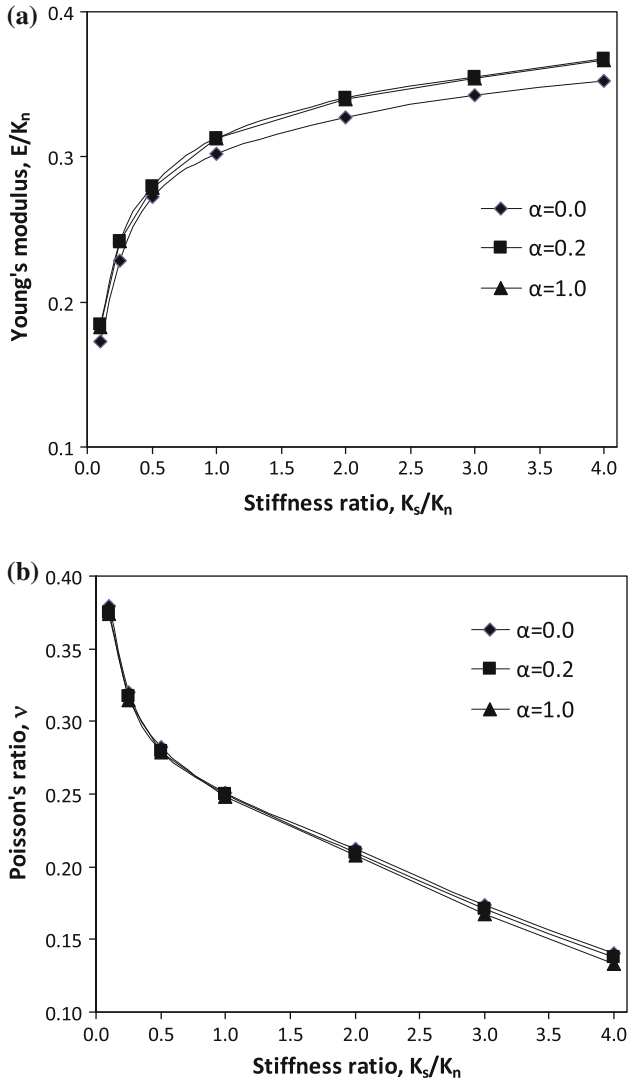

Fig. 3 Effects of the rolling friction coefficient α and the stiffness ratio K_s/K_n on **a** the elastic Young's modulus, and **b** the Poisson's ratio

asymptotically approaches zero as $K_s/K_n \to \infty$, while [34] showed that Poisson's ratio becomes negative for $K_s/K_n > 1$. The differences between the results shown in Fig. 3b and those proposed by [34] are due to the fact that Fig. 3b is for unbonded granular materials, while the predictions by [34] are for bonded particles. In unbonded materials, particles have more freedom to move and volumetric changes can occur more freely than in bonded materials. As noted by [34], negative Poisson's ratios are not likely for granular materials since in most cases $K_s < K_n$. The value $\nu \approx 0.25$ for $K_s/K_n = 1$ from Fig. 3b appears to be more realistic and in agreement with experimental data than the zero Poisson's ratio predicted by [34]. Similar to the Young's modulus E, the rolling friction coefficient α has minimal effects on the Poisson's ratio ν as shown in Fig. 3b.

3.2 Effects of rolling resistance on shear strength and dilatancy

From Fig. 2a, it can be clearly observed that an increase in the rolling friction coefficient α results in higher peak strength. The peak shear stress is more than doubled when α is increased from 0 to 1. The increase in peak shear stress with increasing α indicates that rolling resistance increases the overall frictional resistance of the granular material. The peak shear stress also occurs at higher axial strains for high values of α compared to the stress–strain response at low values of α. In addition, strain softening is more pronounced with a larger drop in post-peak shear stress for high α values than for low α values. Small values of α equal to 0.0, 0.001 and 0.01 do not produce significant changes in the shear stress–strain curves.

As observed in Fig. 2b, as the axial strain is increased, the simulated materials with free rotation or very low rolling resistance ($\alpha = 0$, 0.001 and 0.01) undergo lower volumetric contraction and start to dilate at an earlier stage of $\varepsilon_1 = 1\%$ compared to the materials with high α. The materials with higher rolling resistance ($\alpha = 0.1$ and 1) continue compacting until they start dilating at $\varepsilon_1 = 2\%$. At large axial strains, the dilative volumetric strain increases as the rolling resistance is increased. The increased dilative volumetric changes for the models with high α-values is attributed to the fact that the increased moment between particles caused by the rolling resistance results in the particles being pushed from each other during shearing. On the other hand, in the models with low rolling resistance, the particles are free to jostle around and accommodate each other resulting in smaller dilation. Tordesillas [35] presented similar results indicating that dilatancy increases with increasing rolling resistance.

Figures 4 and 5 summarize the effects of the rolling friction coefficient α on the peak secant friction angle ϕ_s, which is defined as:

$$\sin\phi_s = \left(\frac{\sigma_1 - \sigma_3}{\sigma_1 + \sigma_3}\right)_{\max} \tag{10}$$

For a friction coefficient of $\mu = 0.6$, the secant friction angle ϕ_s continuously increases from about 27° for $\alpha = 0$ to about 39.5° for $\alpha = 1$ (Fig. 4a). The most significant increase in the secant friction angle occurs for $\alpha < 0.2$, and for $\alpha > 0.2$ the change in the friction angle is very small. The variation of the φ as function of α is similar for three values of μ of 0.4, 0.6 and 0.8. In general, for the same α-value, the peak secant friction angle increases with increase in the friction coefficient μ. Figure 4b shows the combined effects of α and the confining stress σ_3 on the secant friction angle ϕ_s. Similar to Fig. 4a, the secant friction angle ϕ_s changes dramatically for $\alpha < 0.2$, and very little change occurs when $\alpha > 0.2$ for all σ_3-values. As expected, for the same value of α, the

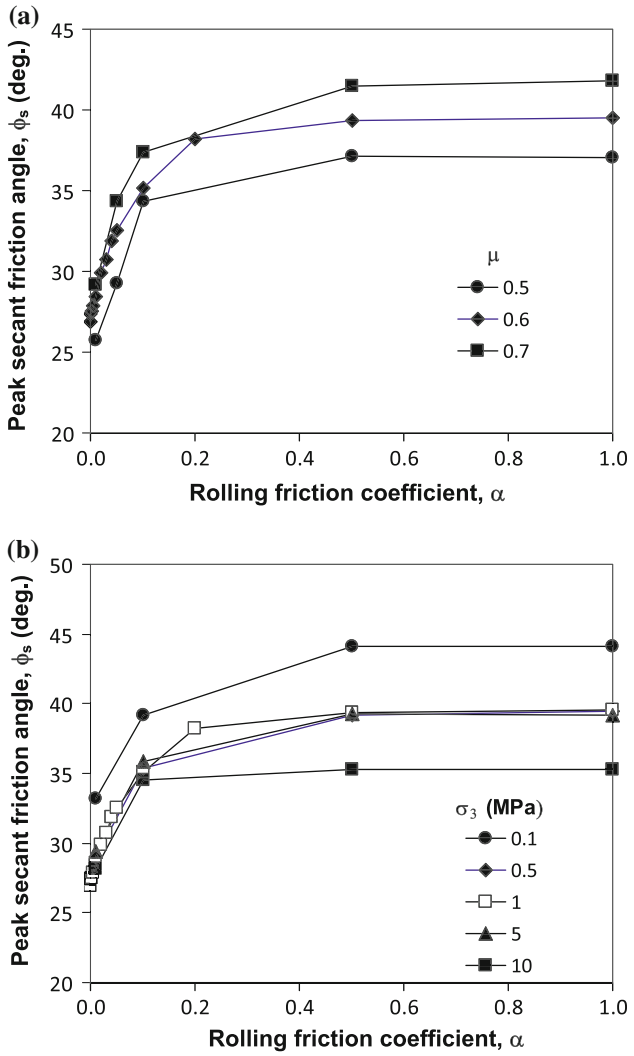

Fig. 4 Effects of the rolling friction coefficient α on peak secant friction angle **a** as function of friction coefficient μ and **b** confining stress σ_3

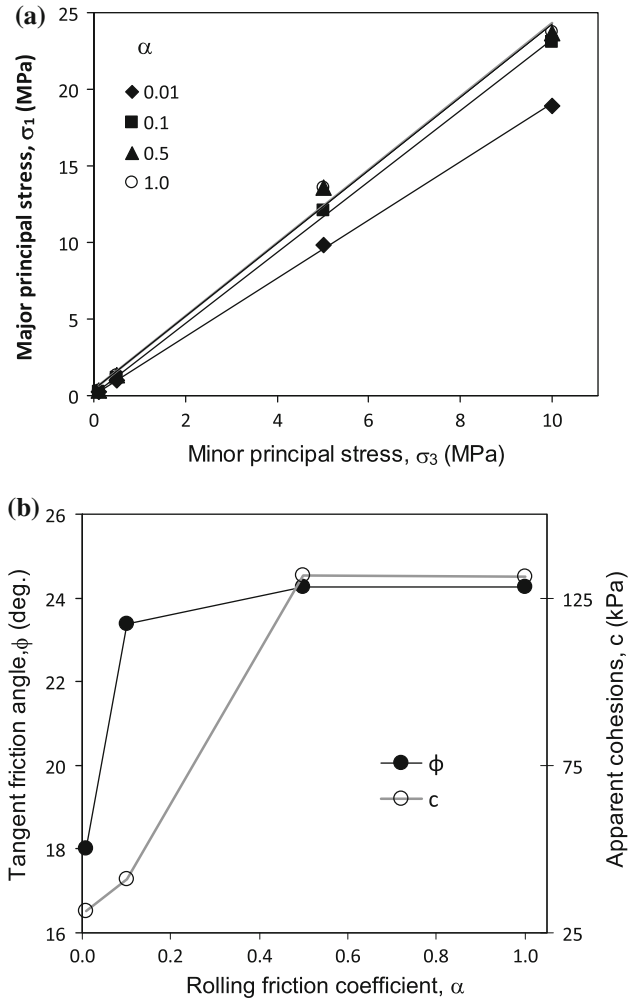

Fig. 5 Effects of the rolling friction coefficient α on **a** peak tangent friction angle **b** apparent cohesion obtained from the linearization of the failure points

secant friction angle ϕ_s decreases with increasing confining stress σ_3.

The effect of rolling friction coefficient α on the tangential friction angle φ is shown in Fig. 5a and b. In Fig. 5a, the tangential friction angle for each value of α is determined from the peak values of σ_1 plotted against the confining stress σ_3. As can be seen, although the failure points can be sufficiently represented by a linear failure criterion with a constant φ, a more accurate representation would require a nonlinear failure criterion. It is evident from Fig. 5a, that φ increases with α, and this variation is shown in Fig. 5b. The tangential friction angle changes rapidly for $\alpha < 0.2$, and little change is observed for $\alpha > 0.2$. As indicated in Fig. 5a, the measured failure points become more nonlinear and deviate more from the linear approximation as α is increased. Due to the linear approximation, an apparent cohesion c is obtained from the linear failure lines. The variation of the apparent cohesion values obtained from Fig. 5a is shown in Fig. 5b, which shows that the change in apparent cohesion occurs more rapidly for $\alpha < 0.5$.

Figure 6 shows the effects of rolling friction coefficient α on the peak dilation angle ψ, which is defined as:

$$\sin\psi = \left(\frac{d\varepsilon_1 + d\varepsilon_3}{d\varepsilon_1 - d\varepsilon_3}\right)_{\max} = \frac{(d\varepsilon_v/d\varepsilon_1)_{\max}}{(d\varepsilon_v/d\varepsilon_1)_{\max} - 2} \tag{11}$$

In general, the dilation angle ψ increases for $\alpha < 0.2$ then decreases afterwards. For instance, for the friction coefficient of $\mu = 0.6$, the dilation angle ψ increases from its lowest value of about 14° for $\alpha = 0$ to a maximum of about 18.5° for $\alpha = 0.2$, then decreases to 15.5° for $\alpha = 1$. The same variation of ψ with respect to α is observed for different values of μ (Fig. 6a) and for different values of σ_3 (Fig. 6b). For the same α-value, the dilation angle increases with increasing μ (Fig. 5a) and decreases with increasing confining stress σ_3 (Fig. 6b).

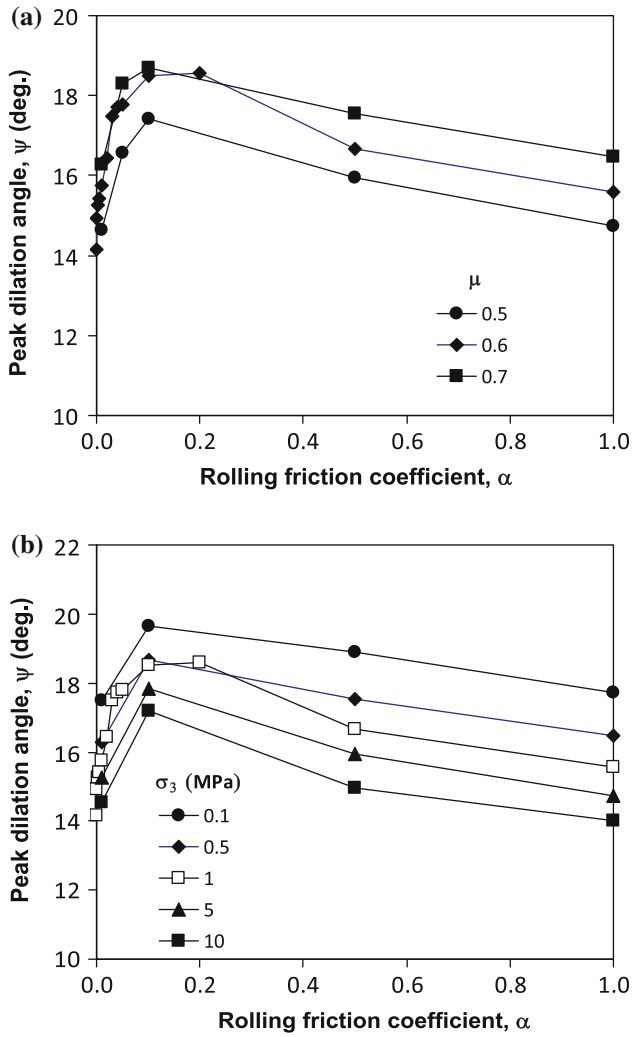

Fig. 6 Effects of the rolling friction coefficient α on peak dilation angle **a** as function of friction coefficient μ and **b** confining stress σ_3

3.3 Effects of rolling resistance on onset of shear band formation

Figure 7 gives typical results from the models showing the displacement vectors at different levels of axial deformation. The value of rolling friction coefficient is $\alpha = 0.1$ for the figures shown. It is observed at the initial stage (Fig. 7a) that the displacement field appears to be reasonably uniform. With an axial strain of 0.02 (Fig. 7b), the displacement field still remains relatively uniform with the sample undergoing vertical compression and lateral expansion. As the axial strain is increased, the displacements begin to localize into two conjugate shear bands at the center of the sample (Fig. 7c). This small localized zone of deformation is noticeable even before the peak shear stress has been reached. However, the small bands of deformation are short-lived, and they vanish and re-appear as shearing continues prior to the peak shear strength. Shortly after the peak, the small conjugated shear bands coalesce and suddenly turn to form a single contiguous shear band (Fig. 7d). At $\varepsilon_1 = 0.1$, the shear band is fully developed and spans the entire height of the sample (Fig. 7e). With increasing axial deformation, the shear band becomes narrower and more distinct. This trend was also observed experimentally by [36]. The results also suggest that the use of rigid top and bottom walls and semi-rigid laterals walls as boundaries does not prevent the formation of shear band within the sample, although they may restrain further shear band development.

Figure 8 shows the influence of rolling resistance on the formation of shear band in the simulation of biaxial tests on granular materials. Snapshots of the displacement fields for $\alpha = 0, 0.001, 0.01, 0.1$ and 1.0 are shown. In all the figures, the displacement vectors are shown at the residual shear state and axial strain of $\varepsilon_1 = 0.1$. The confining pressure, porosity, contact friction angle and other model parameter values are again the same for all α-values. It can be seen in these figures that there are no clear indications of shear band formation even at large deformation for low values of $\alpha = 0$ and 0.001 (Fig. 8a, b). Iwashita and Oda [25] reported that shear band does not clearly form in the case of free rotation as the strain concentration changes from step to step so quickly that the overall distribution of deformations looks uniform. In contrast, distinct shear bands are observed in the cases where $\alpha = 0.01, 0.1$ and 1. Figure 8 clearly proves the importance of rolling resistance in promoting shear band formation in granular materials.

3.4 Effect of rolling resistance on shear band orientation

To further quantify the effects of rolling resistance on shear band formation, the orientations of the shear bands were directly measured from the models. Only the cases with distinctly observable shear bands were included in the analysis. It was observed that the shear bands were not always completely straight along its length, but sometimes tend to bend towards the corners of the four edges of the samples. Thus, the shear bands were measured along the straight line portions of the shear bands in the middle of sample. The orientations of the shear band plane θ_m from the models were measured from the horizontal axis, and these are shown against α in Fig. 9.

The measured shear band inclinations are compared with three theoretical shear band orientations. These are the Mohr-Coulomb orientation θ_{MC} and Roscoe orientation θ_R [37] which are, respectively, the upper and lower bound values of the orientation of the shear band plane measured from the horizontal axis:

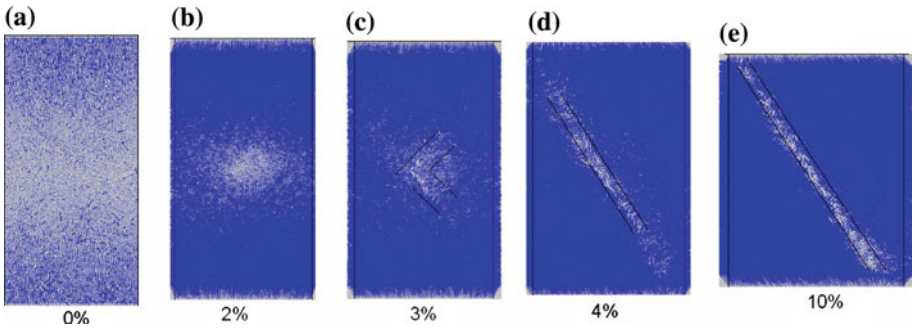

Fig. 7 Development of shear band with increasing axial strain ($\alpha = 0.1$)

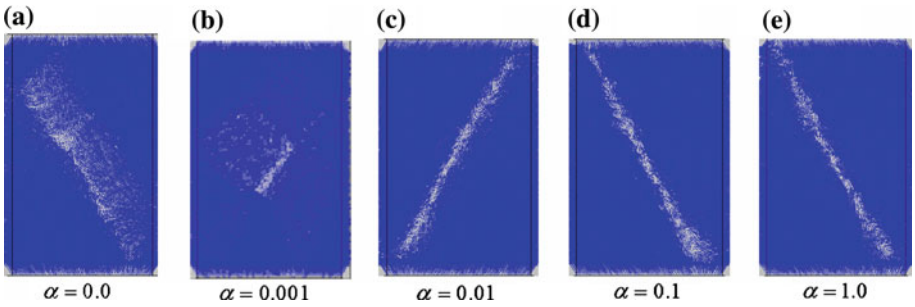

Fig. 8 Effects of the rolling friction coefficient α on strain localization ($\varepsilon_1 = 0.1$)

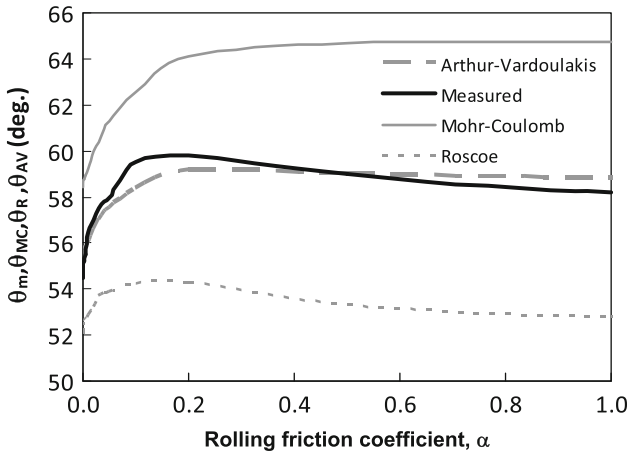

Fig. 9 Effects of the rolling friction coefficient α on shear band orientation

$$\theta_{MC} = 45 + \frac{\phi}{2}, \quad \theta_R = 45 + \frac{\psi}{2} \tag{12}$$

The third orientation is the Arthur-Vardoulakis orientation θ_{AV} from [38,39] and corresponds to the average inclination between the Mohr-Coulomb and Roscoe orientations:

$$\theta_{AV} = 45 + \frac{1}{2}\left(\frac{\phi + \psi}{2}\right) \tag{13}$$

Figure 9 shows the variation of the measured shear band orientation θ_m from the models against the rolling friction coefficient α. It is observed that θ_m first increases with increasing value of α. The measured shear band inclination angle for free rotation is about $\theta_m = 54.5°$, then it reaches its highest value at about 60° at $\alpha = 0.25$ and decreases thereafter to $\theta_m = 58°$ for $\alpha = 1.0$. Figure 9 also shows the Mohr-Coulomb, Roscoe and Arthur-Vardoulakis shear band orientations from Eqs. (12) and (13) using the actually measured peak friction angle ϕ and dilation angle ψ from the models. The measured shear band orientations are closest to the Arthur-Vardoulakis predictions. The Mohr-Coulomb orientation over predicts while the Roscoe orientation under predicts the measured shear band inclinations. Similar variation of shear band orientation as function of α were observed for different particle sizes and values of the friction coefficient μ and confining stress σ_3.

3.5 Effect of rolling resistance on shear band thickness

Most authors define the shear band thickness by the number of particles that span the shear band width. Oda and Kazama [21], Arthur et al. [38], and Mulhaus and Vardoulakis [40] each reported that the width of shear band is 8–20 times the mean diameter D_{50}. In the following, the width of the shear band is also normalized with respect to the mean diameter D_{50} of the particles. Figure 10 shows the shear band thicknesses from the models as function of the rolling friction coefficient α. The width of the shear band decreases significantly with a value of about 18 times the mean particle diameter D_{50} for $\alpha = 0$, to 12 for $\alpha = 0.1$ and 10 for $\alpha = 1.0$. The shear band width decreases rapidly with increasing α for $\alpha < 0.1$. The results indicate that when particle rotation is hindered by high rolling resistance, the buckling of column of particles occur in a narrower zone producing a thinner shear band. On the other hand, when particles are free to rotate and move around due to low rolling resistance, the buckling occurs over a wider zone resulting in a wider shear band.

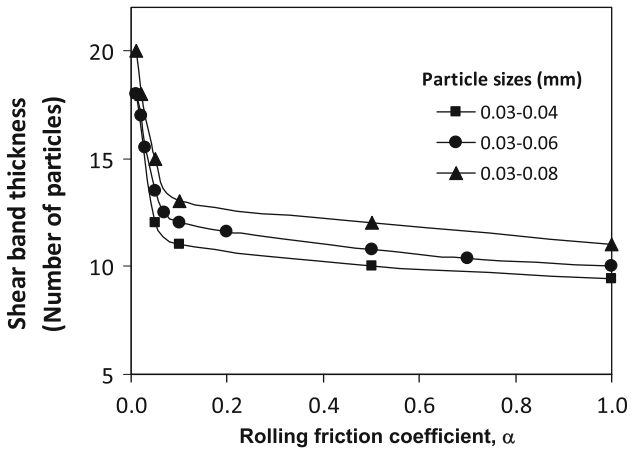

Fig. 10 Effects of the rolling friction coefficient α on shear band thickness for different ranges of particle sizes

This is in agreement with the observation of [18]. As can be seen in Fig. 10, the width of the shear band normalized with respect to mean diameter D_{50} is not unique, and the normalized shear band thickness increases with increasing value of D_{50}. It appears that another measure of the grain size diameter is needed to achieve a unique normalized shear band thickness as function of α.

3.6 Micromechanical observations

The development of force chains is a common feature in the stress–strain response of granular materials [5,28,40]. Force chains are quasilinear arrangements of group of particles by which compressive loads are transmitted. Their average orientations are more or less sub-parallel to the major principal stress, and they form solid column-like structures which provide resistance to shear and serve as the load-bearing network responsible for the strength and stability of granular materials. When a granular assembly is loaded and sheared, force chains form, rotate and collapse as the shearing progresses. Force chains develop anisotropically during shearing due to the fact that not all particles form equal parts of the network of force chains. As the shearing proceeds beyond peak shear stress, the major force chains reorganize until they can longer provide the best possible pathway for force transmission.

The reconfiguration of the network of force chains during biaxial shearing of the modeled granular material is shown in Fig. 11. Before failure, the network of force chains is dense and evenly distributed throughout the volume of the granular material. Once the peak shear stress is reached, the density of the number of force chains is reduced inside the shear band, and there are fewer particle-to-particle contacts available within the shear band to transmit the loads. As the number of particle-to-particle contacts are decreased, the frictional resistance between particles may be exceeded causing the force chain to collapse. As a result, the load carrying capacity of the granular material is reduced and strain softening occurs [41].

Figure 12 shows a comparison of the force chains for the model with $\alpha = 0$, 0.2 and 1, all at an axial strain of $\varepsilon_1 = 0.1$. The model with no rolling resistance shows that the granular material is able to retain a more uniform force chain distribution during shearing due to the ability of the particles to move freely and form new contacts during shearing. The force chains are oriented more uniformly and the average force chain direction is generally sub-parallel to the major principal stress direction. Because of the ability of the particles to rotate and move freely in the absence of rolling resistance, collapse of the network of force chains and the formation of a shear band are prevented. In contrast, the reduction in the number particle-to-particle contacts inside the shear band is very visible in the models with α equal to 0.2 and 1. Large contact forces, represented by thicker lines, appear due to the reduced number of contacts supporting the load. The force chain directions inside the band are no longer uniformly distributed. Also, the average force chain direction within the shear band are no longer sub-parallel but deviate from the major principal stress direction. Such deviation produces high rotational moment and stress gradients within the shear band. As a result, the force chains may collapse and cause further instability of the granular mass. Rotational resistance increases the shear strength of the granular material, but the collapse of the force chains and the buckling of columns of grains cause instability and strain localization. As a result, the instability is accompanied by larger reduction in load carrying capacity than in the case of no rolling resistance.

The roles of column bucking and particle rotation are clearly shown in Fig. 13 for the models with $\alpha = 0, 0.2$ and 1 at $\varepsilon_1 = 0.1$. In the case of $\alpha = 0$, the colored columns used to track the movement of particles slightly bends and curves at different locations along the column. In contrast, in the case of $\alpha = 0.2$ and 1, the colored columns have clearly buckled at one location within the shear band. The columns buckled despite the fact that the lateral boundaries are constrained by confining stresses σ_3. Rolling resistance endows the columns with bending stiffness which increases the overall shear strength of the granular material. However, the columns enhance instability due to the tendency of the columns to buckle during loading. In contrast, in the case of low or no rolling resistance, particles are free to move and are unable to form columns with sufficient rigidity to buckle locally.

It is observed in Fig. 13 that for $\alpha = 0$, the particles rotate widely over the granular assembly at all stages of deformation (as shown in the inset figure by the radial line drawn from the center of each particle). The particles tend to have a uniform distribution of rotation with

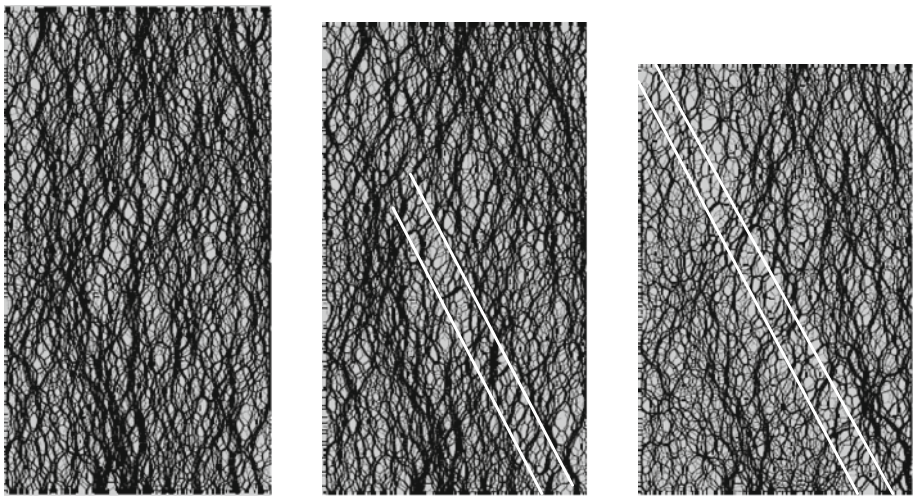

(a) ε_1=2.8% (pre-failure) **(b)** ε_1=3.2% (at failure) **(c)** ε_1=10% (post-failure)

Fig. 11 Development of force chains at different levels of axial strain ($\alpha = 0.2$)

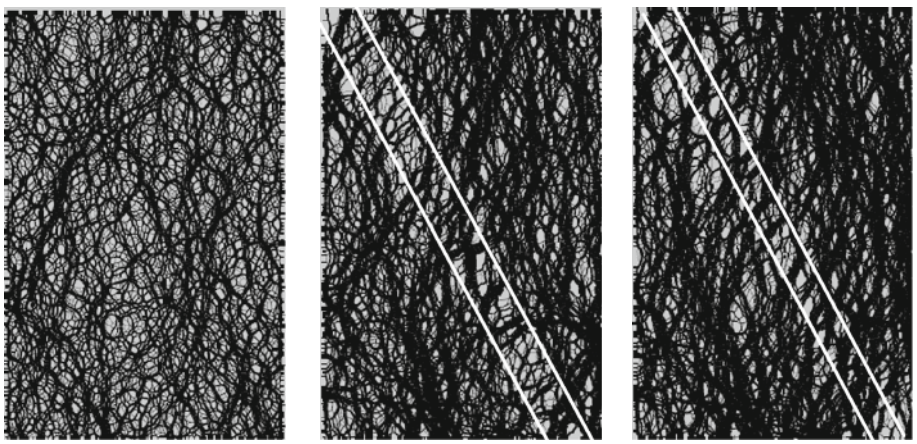

(a) α=0 **(b)** α=0.2 **(b)** α=1.0

Fig. 12 Development of force chains for $\alpha = 0$, 0.2 and 1($\varepsilon_1 = 0.1$)

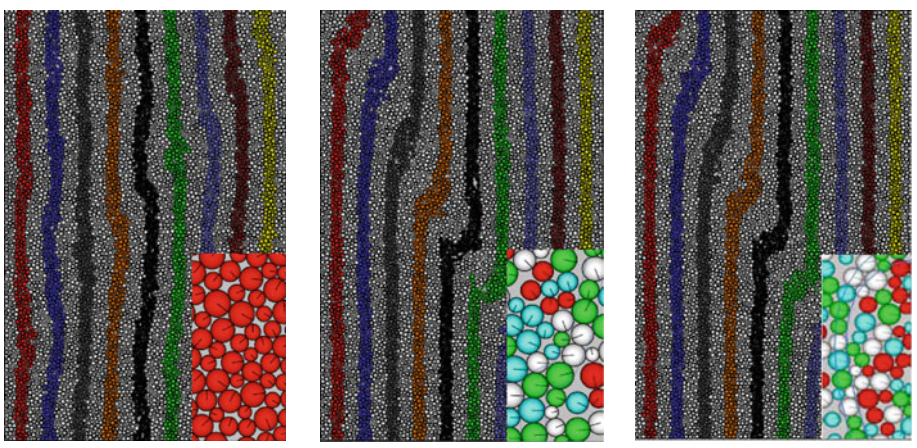

(a) α=0 **(b)** α=0.2 **(c)** α=1.0

Fig. 13 Buckling of columns of particles and particle rotation (*insets*) for $\alpha = 0$, 0.2 and 1($\varepsilon_1 = 0.1$)

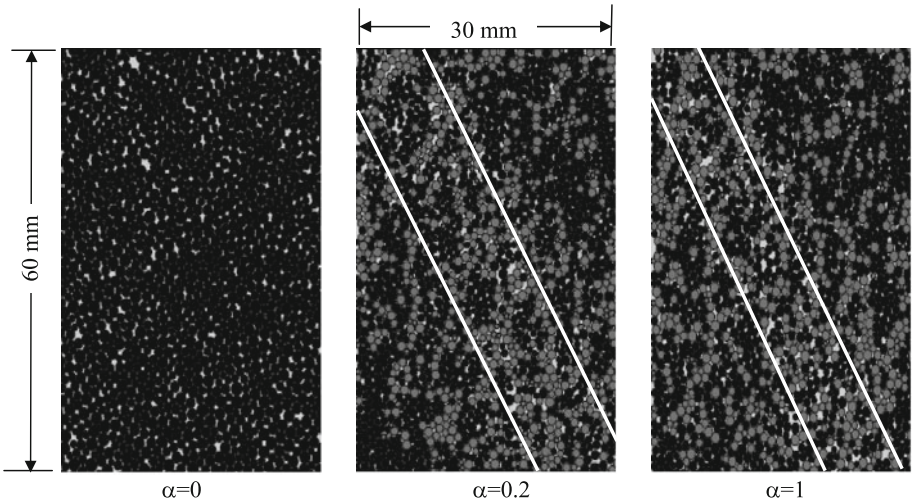

Fig. 14 Development large voids within shear band for $\alpha = 0, 0.2$ and $1(\varepsilon_1 = 0.1)$

the exception of the central zone which shows slightly more highly rotated particles. However, rotations are distributed rather uniformly in both clockwise and counter clockwise directions. For $\alpha = 0.2$ and 1, the particles show only very small rotations before the shear band is formed. Once the deformations have localized, particle rotation occurs extensively within shear band while no significant rotations are observed for the particles outside the shear band. As a result, the buckling of the columns and the shear band formation are accompanied by large gradients in the magnitude of particle rotations. Similar observations were made by [15].

Another important observation is that particle rotation in the presence of rolling resistance is associated with the formation of large voids within the shear band (Fig. 14). This non-uniform void distribution can be seen more clearly in the enlargement of the leftmost and topmost 1/4th (or $3 \times 6\,\text{cm}^2$) portion of the sample. For $\alpha = 0.2$ and 1, nearly uniform voids are formed outside the band while large voids are formed inside the band. In comparison, for the case of no rolling resistance, the void distribution is nearly uniform outside and inside the shear band. The occurrence of areas of large voids in the case where particles have rolling resistance is attributed to the fact that particles in the presence of rotational moments tend to push each other apart. This causes the granular assembly to expand and increase the overall volume locally. In comparison, in the case of free rotation, particles are free to move locally and accommodate each other resulting in a more uniform distribution of porosity.

4 Conclusions

In this paper, the effects of rolling resistance on the mechanical and shear banding behavior of granular materials under biaxial loading conditions were investigated extensively using DEM. The conventional DEM was modified by the implementation of a user-defined model for rolling resistance in PFC. The PFC models were also tested under a range of macro-mechanical parameters and boundary conditions. The following specific conclusions can be drawn from the investigation:

1. The initial slopes of the $(\sigma_1 - \sigma_3)$ vs. ε_1, and the ε_v vs. ε_1 curves, and the initial deformation moduli (i.e., Young's modulus E and Poisson's ratio ν) were relatively unaffected by rolling friction coefficient α. In contrast, both E and ν were strongly influenced by the stiffness ratio K_s/K_n, with E increasing with increasing K_s/K_n ratio, and ν decreasing with increasing K_s/K_n ratio. For K_s/K_n =1, which is the most commonly used assumption in particulate modeling of granular materials, $\nu \approx 0.25$. This value is more realistic and in better agreement with experimental results than the value of $\nu = 0$ obtained by [34] for bonded granular material for $K_s/K_n = 1$.
2. The peak secant and tangent friction angles increased with increasing value of the rolling friction coefficient α. The peak secant friction angle increased by about $8-12°$ when α was increased from 0 to 1 depending on the value of μ and σ_3. The peak tangent friction angle increased by about 6° when α was increased from 0 to 1 for $\mu = 0.6$. The most significant increase occurred for $\alpha < 0.2$, while very small changes occurred for $\alpha > 0.2$. The same trend in the variation of the secant and tangent friction angles with respect to α was observed for different values of the friction coefficient μ and confining stress σ_3.
3. The dilation angle ψ also increased by about 5° with increasing α for $\alpha < 0.2$ and decreased thereafter by about 2° for $\alpha > 0.2$. The lowest value of ψ was obtained for the case of free rotation. The same trend

in the variation of ψ with respect to α was observed for different values of the friction coefficient μ and confining stress σ_3.

4. Rolling resistance enhanced shear band formation in granular materials with more distinct and fully localized zones at residual strains for values of $\alpha > 0.1$ and more diffused deformation and less clear shear bands for values of $\alpha < 0.01$.
5. The measured shear band orientation θ_m, measured from the σ_3-axis, increased from $\theta_m \approx 55°$ for $\alpha = 0$ to $\theta_m \approx 60°$ for $\alpha \approx 0.15$ then decreased slightly to $\theta_m \approx 58°$ for $\alpha = 1$. Regardless of the value of α, the orientation of the shear band was closest to the Arthur-Vardoulakis orientation proposed by [38,39]. The Mohr-Coulomb and the Roscoe orientations were significantly above and below, respectively, the measured orientations.
6. The shear band thickness decreased with increasing rolling resistance, with a thickness of about 18 times the mean particle diameter D_{50} for $\alpha = 0$, 12 for $\alpha = 0.1$, and about 10 for $\alpha = 1$. The shear band thickness decreased rapidly with α for $\alpha < 0.1$. Normalizing the shear band thickness with respect to the D_{50} grain size does not provide a unique measure of the shear band thickness as function of α.
7. The configuration of force chain structures depended strongly on the magnitude of rolling resistance. In the absence of rolling resistance, the force chains were oriented more uniformly and the average force chain direction was generally sub-parallel to the major principal stress direction. With increasing rolling friction coefficient above 0.2: (a) the number of particle-to-particle contact decreased, (b) larger contact forces appeared due to the reduced number of contacts supporting the load, and (c) the average force chain direction within the shear band deviated from the major principal stress direction.
8. Due to the deviation of the force chain directions from the major principal stress direction, high rotational moments and stress gradients were produced within the shear band. Instability and strain localization occurred due to the changes in configuration of the force chains and the presence of rotational moments and stress gradients.
9. Due to the rotational resistance, columns of particles formed during loading of the granular material. These columns increased the shear strength but enhanced instability due to the tendency of the columns to buckle during loading despite the application of confining stresses at the lateral boundaries. In contrast, particles were free to move and were unable to form columns in the case of low or no rolling resistance. As a result, instability in the case of high rolling resistance was accompanied by larger reduction in load carrying capacity than in the case of low or no rolling resistance.
10. In the case of $\alpha = 0$, particles rotated widely over the granular assembly at all stages of deformation. In comparison, in the case of $\alpha > 0.2$, the particles showed only very small rotations before the shear band was formed. Once deformations have localized, particle rotation occurred extensively within the shear band while no significant rotations were observed for the particles outside the shear band. As a result, the shear band formation was accompanied by gradients in the magnitude of particle rotations.
11. Particle rotation within the shear band in the presence of rolling resistance was associated with the formation of non-uniform void distribution within the shear band. Paradoxically, large voids were created at the same time that the shear band width decreased as α is increased. The occurrence of areas of large voids where particles have high rolling resistance was attributed to the fact that particles, in the presence of rotational moments, tended to push each other apart. This caused the granular assembly to expand and increase the porosity locally. In comparison, particles were free to move and accommodate each other, resulting in more uniform void distribution, in the case of low or no rolling resistance.

References

1. Oda, M., Konishi, J., Nemat-Nasser, S.: Experimental micromechanical evolution of strength of granular materials: effects of particle rolling. Mech. Mater. **1**, 269–283 (1982)
2. Cundall, P.A.: A discrete numerical model for granular assemblies. In: Proceedings of ISRM Symposium, vol. 2, pp. 129–136. Nancy, France (1971)
3. Cundall, P.A., Strack, O.L.: A discrete numerical model for granular assemblies. Geotechnique **29**, 47–65 (1979)
4. Bardet, J.P., Proubet, J.: Numerical simulation of localization in granular materials. In: Proceedings of EMD/ASCE Conference, pp. 1269–1273. Columbus, Ohio (1991)
5. Iwashita, K., Oda, M.: Micro-deformation mechanism of shear banding process based on modified distinct element method. Powder Tech. **109**, 192–205 (2000)
6. Hu, N., Molinari, J.F.: Shear bands in dense metallic granular materials. J. Mech. Phys. Solids **52**, 499–531 (2004)
7. Gardiner, B., Tordesillas, A.: Micromechanics of shear bands. Int. J. Solids Struct. **41**, 5885–5901 (2004)
8. Mandel, J.: Conditions de stabilité et postulat de Drucker. In: Proceedings of IUTAM Symposium on Rheology and Soil Mechanics, pp. 58–68 (1966)
9. Rudnicki, J.W., Rice, J.R.: Conditions for the localization of deformation in pressure-sensitive dilatant materials. J. Mech. Phys. Solids **23**, 371–394 (1975)
10. Vardoulakis, I.: Equilibrium theory of shear bands in plastic bodies. Mech. Res. Comm. **3**, 209–214 (1976)
11. Newland, P.L, Allely, B.H.: Volume changes in drained triaxial tests on granular materials. Géotechnique **7**(1), 17–34 (1957)
12. Rowe, P.W.: The stress-dilatancy relation for static equilibrium of an assembly of particles in contact. Proc. R. Soc. Lond. Ser. A **269**, 500–527 (1962)

13. Schofield, A., Wroth, C.P.: Critical State Soil Mechanics. McGraw-Hill, London (1967)
14. Mitchell, J.K.: Fundamentals of Soil Behavior. Willey, New York (1976)
15. Jiang, M.J., Haris, D.A.: Novel discrete model for granular material incorporating rolling resistance. Comput. Geotech. **32**(5), 340–357 (2005)
16. Bardet, J.P.: Observations on the effects of particle rotations on the failure of idealized granular materials. Mech. Mater. **18**, 159–182 (1994)
17. Wang, J.F., Gutierrez, M., Dove, J.E.: Effect of particle rolling resistance on interface shear behavior. In: Proceedings of 17th ASCE Engineering Mechanics Conference, pp. 56–63 (2004)
18. Oda, M., Iwashita, K.: Study on couple stress and shear band development in granular media based on numerical simulation analyses. Int. J. Eng. Sci. **38**(15), 1713–1740 (2000)
19. Bardet, J.P., Proubet, J.: The structure of shear bands in idealized granular materials. Appl. Mech. Rev. **45**(3), 118–122 (1992)
20. Oda, M., Kazama, H., Konishi, J.: Effects of induced anisotropy on the development of shear bands in granular materials. Mech. Mater. **28**(1-4), 103–111 (1998)
21. Oda, M., Kazama, H.: Microstructure of shear bands and its relation to the mechanisms of dilatancy and failure of dense granular soils. Geotechnique **48**(1-4), 465 (1998)
22. Tordesillas, A., Shi, J.: Micromechanical analysis of failure propagation in frictional granular materials. Int. J. Numer. Anal. Method Geomech. **33**, 1737–1768 (2009)
23. Itasca Consulting Group.: Particle Flow Code in 2D (PFC-2D): User's Manual, Version 4.0. Minneapolis, Minnesota (2008)
24. Bardet, J.P., Huang, Q.: Rotational stiffness of cylindrical particle contacts. In: Proceedings of Powders and Grains Conference, pp. 39–43 (1993)
25. Iwashita, K., Oda, M.J.: Rolling resistance at contacts in the simulation of shear band development by DEM. J. Eng. Mech. **124**(3), 285–292 (1998)
26. Sakaguchi, H., Ozaki, E., Igarashi, T.: Plugging of the flow of granular materials during discharge from a silo. Int. J. Mod. Phys B **7** (9–10), 1949–1963 (1993)
27. Jiang, M.J., Yu, H.-S., Harris, D.: Kinematic variables bridging discrete and continuum granular mechanics. Mech. Res. Comm. **33**, 651–666 (2006)
28. Jiang, M.J., Leroueil, S., Zhu, H.-H., Yu, H.-S., Konrad, J.M.: Two-dimensional discrete element theory for rough particles. Int. J. Geomech. ASCE. **9**(1), 20–33 (2009)
29. Jiang, M.J., Yu, H.-S., Harris, D.: Bond rolling resistance and its effect on yielding of bonded granulates by DEM analyses. Int. J. Numer. Anal. Method Geomech. **30**(7), 723–761 (2006)
30. Luding, S.: Cohesive, frictional powders: contact models for tension. Granul. Matter **10**(4), 235–246 (2008)
31. Bartels, G., Unger, T., Kadau, D., Wolf, D.E., Kertesz, J.: The effect of contact torques on porosity of cohesive powders. Granul. Matter **7**(3), 139–143 (2005)
32. Wang, Y.C., Alonso-Marroquin, F.: A finite deformation method for discrete modeling: particle rotation and parameter calibration. Granul. Matter **11**(5), 331–343 (2009)
33. Ng, T.T.: Input parameters of discrete element methods. J. Eng. Mech. **132**(7), 723–729 (2006)
34. Bathurst, B.J., Rothenburg, L.: Note on a random isotropic granular materials with negative Poisson's ratio. Int. J. Eng. Sci. **26**(4), 373–383 (1988)
35. Tordesillas, A.: Force chain buckles, unjamming transitions and shear banding in dense granular materials. Philos. Mag. **87**, 4987–5016 (2007)
36. Wang, Q., Lade, P.V.: Shear banding in true triaxial tests and its effect on failure in sand. J. Eng. Mech. **127**(8), 754–761 (2001)
37. Roscoe, K.H.: The influence of strain in soil mechanics. Géotechnique **20**(2), 129–170 (1970)
38. Arthur, J., Dunstan, T., Al-Ani, Q., Assadi, A.: Plastic deformation and failure in granular media. Geotechnique **27**(1), 53–74 (1977)
39. Vardoulakis, I.: Shear band inclination and shear modulus of sand in biaxial tests. Int. J. Numer. Anal. Methods Geomech. **4**(2), 103–119 (1980)
40. Muhlhaus, H.B., Vardoulakis, I.: The thickness of shear bands in granular materials. Geotechnique **37**, 271–283 (1987)
41. Tordesillas, A., Peters, J.F., Muthuswamy, M.: Role of particle rotations and rolling resistance in a semi-infinite particulate solid indented by a rigid flat punch. ANZIAM J. **46**, 260–275 (2005)